RSC Advances

PAPER

View Article Online
View Journal | View Issue

Cite this: *RSC Adv.*, 2025, **15**, 40558

Effectiveness of a novel C4-substituted heterocyclic organic pyrazolone as a corrosion inhibitor for mild steel in 1.0 M HCl: electrochemical, surface analytical and theoretical studies

Youssef Adnan,[a] Younesse Ait Elmachkouri,[a] Noureddine Idlahoussaine,[a] Ezaddine Irrou,[a] Brahim El Ibrahimi, *[ab] Az-Eddine El Mansouri,[c] Murat Yilmaz,[d] Hassan Ouachtak,[ab] Nada Kheira Sebbar,[ab] Mohamed Labd Taha,[a] Abdul Shaban[e] and Abdelaziz Ait Addi[a]

This study investigates the corrosion inhibition performance of a novel C4-substituted pyrazolone-based heterocyclic compound, namely 3-(5-methyl-3-oxo-2,3-dihydro-1*H*-pyrazol-4-yl)-3-phenylpropanoic acid (**C4-PRZ-1**), on mild steel (MS) in a 1 M hydrochloric acid (HCl) environment. Electrochemical impedance spectroscopy (EIS) and potentiodynamic polarization (PDP) methods were employed to evaluate the inhibitor's protective capabilities. The effects of varying inhibitor concentrations and temperature on inhibition efficiency were systematically examined. Results demonstrated that increasing the inhibitor concentration improved corrosion protection, with a maximum efficiency of 85% observed at 5.0 mM. Furthermore, raising the temperature from 298 to 328 K caused a decrease in the inhibitive efficiency of the examined compound. The adsorption behavior of **C4-PRZ-1** on the MS surface followed the Langmuir's isotherm model. Thermodynamic parameters associated with the adsorption process were determined to provide further insight into the inhibition mechanism. Surface morphology and elemental composition analyses using scanning electron microscopy (SEM) and energy-dispersive spectroscopy (EDS) confirmed the formation of a protective film on the steel surface. Additionally, density functional theory (DFT) calculations were conducted to explore the electronic interactions, particularly the charge transfer between chloride ions and the steel substrate. Monte Carlo simulations, in conjunction with simulated annealing algorithms (SAA) and adsorption locator techniques, further elucidated the molecular interactions between the inhibitor and the metal surface, supporting the experimental findings.

Received 2nd May 2025
Accepted 10th October 2025

DOI: 10.1039/d5ra03090k

rsc.li/rsc-advances

1. Introduction

Mild steel, characterized by a relatively low carbon content (typically between 0.05% and 0.25%), exhibits greater ductility and softness compared to high-carbon steel. These properties, combined with its low cost, good machinability, and excellent weldability, make it a widely utilized material in various industrial applications, particularly in construction and manufacturing sectors.[1–3] Nevertheless, it is exceedingly susceptible to corrosion, particularly in acidic environments like those used in acid pickling. To protect mild steel from corrosion in such conditions, inhibitors are considered crucial.[4,5] Organic compounds have become widely recognized for their capacity to prevent the corrosion of mild steel and iron, demonstrating effectiveness across a range of corrosive environments.[4–6] Hydrochloric acid, commonly used in industrial processes, including pickling, is particularly corrosive.[7] As a result, corrosion inhibitors are often the best solution to reduce the rate of metal dissolution in acidic environments. A wide range of organic compounds has been effectively employed as corrosion inhibitors within the industrial acid treatment processes.[8–10]

[a]*Laboratory of Organic Chemistry and Physical Chemistry, Faculty of Science, Ibnou Zohr University, PB 8106, Agadir, Morocco. E-mail: brahimmhm@gmail.com*

[b]*Department of Applied Chemistry, Faculty of Applied Science, Ibnou Zohr University, PB 86153 Ait Melloul, Agadir, Morocco*

[c]*Laboratory of Biotechnology, Agrifood, Materials, and Environment, Faculty of Science and Technology Mohammedia, Hassan II University of Casablanca, BP 146, Mohammedia 20650, Morocco*

[d]*Osmaniye Korkut Ata University, Bahçe Vocational School, Department of Chemistry and Chemical Processing Technologies, Osmaniye, 80000, Turkiye*

[e]*Institute of Materials and Environmental Chemistry, Research Centre for Natural Sciences, Bp., Hungary*

The inhibition efficiency, adsorption behavior, and associated mechanisms are affected by various factors, including the structural and electronic features of the inhibitor, surface properties, and operational conditions such as pressure, temperature, flow rate, and the composition of the corrosive environment.[11–15] Organic corrosion inhibitors can be broadly classified into several categories based on their chemical structures and functional groups. These include heterocyclic compounds (*e.g.*, triazoles, imidazoles, and pyridines), Schiff bases, amines, surfactants, and polymeric inhibitors. Typically, organic compound, their effectiveness is primarily attributed to the presence of electronegative atoms, such as nitrogen (N), sulfur (S), and oxygen (O) characterized by high basicity and electron density, are efficient at resisting corrosion.[16,17] Nitrogen and oxygen atoms, in particular, are key in adsorbing onto metal surfaces, preventing corrosion by blocking access to active sites.

In recent years, the development and application of green corrosion inhibitors-typically derived from renewable natural sources such as plant extracts, amino acids, and biodegradable surfactants have gained significant attention due to their low toxicity and environmental compatibility,[18] but in some cases, green inhibitors may not match the efficiency of well-optimized synthetic inhibitors, especially under harsh conditions (high temperatures, high acid concentrations).[19] In addition, natural compounds may degrade over time or under exposure to light, oxygen, or high temperatures.[20]

The effectiveness of these synthetic inhibitors compounds as inhibitors is contingent upon various aspects, including the availability of lone electron pairs, the properties of π-electrons, and the electron density surrounding oxygen and nitrogen atoms.[21–24] Inhibitors containing both nitrogen and sulfur generally show greater corrosion resistance compared to those that only contain one of these elements.[25–27] In the presence of chloride ions (Cl^-), cationic organic inhibitors can provide enhanced corrosion protection due to a synergistic effect onto the metal.[11,12,28,29]

Numerous studies have employed methods such as potentiodynamic polarization (PDP), electrochemical impedance spectroscopy (EIS), and surface characterization techniques like SEM-EDS to explore the corrosion inhibition performance of pyrazolone compounds.[30–33] Additionally, quantum chemical calculations and surface analysis provide detailed insights into how these inhibitors bond to and interact with metal surfaces.[30–32]

According to the literature, several research groups have synthesized pyrazolic-based derivatives[34–37] and evaluated their efficiency as corrosion inhibitors. Among them, Rashid *et al.*[38] developed new effective inhibitors based on pyrazolic cores (I, Scheme 1). This compound was tested on mild steel in 1 M HCl solution using electrochemical methods and weight loss measurements. They observed that the inhibition efficiency increased with both temperature and concentration of compound I. The maximum inhibition efficiency of 89.5% was achieved at 60 °C and 400 ppm concentration. This inhibitor obeys the Langmuir adsorption isotherm. Similarly, in 2023, Ashmawy *et al.*[39] prepared C4-substituted pyrazolones bearing a hydrazone function with a sulfonamide group (II and III, Scheme 1) and studied them as corrosion inhibitors for mild steel in 1.0 M HCl solutions at 298–323 K by gravimetric, electrochemical, scanning electron microscopy, and quantum chemical calculations. The inhibition efficiencies of the studied compounds ranged from 76.99 to 96.65%, also following the Langmuir adsorption isotherm. In the same context, El Defrawy *et al.*[40] reported that C4-substituted pyrazolone derivatives (IV and V, Scheme 1) inhibited both general and pitting corrosion of carbon steel in 0.5 M HCl solution. These studies were conducted using galvanostatic techniques, potentiodynamic anodic polarization, and electrochemical impedance spectroscopy (EIS). The inhibitory action of these derivatives was attributed to their adsorption on the steel surface according to the Freundlich isotherm. Inspired by the structures of these molecules (I–V, Scheme 1), which demonstrate significant corrosion inhibition efficiency, we have synthesized a single C4-substituted pyrazolic derivative (**C4-PRZ-1**) and evaluated its performance as a corrosion inhibitor for mild steel in acidic solutions.

C4-substituted pyrazolone derivatives have recently gained attention as highly efficient organic inhibitors for corrosion protection across a range of industrial applications. The mechanism behind their effectiveness is typically ascribed to the adsorption of the inhibitor molecules onto the metal surface, forming a protective barrier that prevents corrosion from progressing.

The primary objective for researchers in this field is to identify new inhibitors that can minimize the harmful effects of pickling acids while also being low in toxicity and cost-effective.[41] In this view, the current research aims to explore the corrosion-inhibiting efficacy of a novel heterocyclic compound, 3-(5-methyl-3-oxo-2,3-dihydro-1*H*-pyrazol-4-yl)-3-phenylpropanoic acid (**C4-PRZ-1**), in an acidic medium. Specifically, it focuses on evaluating how effectively **C4-PRZ-1** reduces the corrosion of MS in a 1.0 M HCl solution. EIS, SEM, and PDP are the primary methods used to assess the compound's ability to inhibit corrosion.

2. Materials and methods

2.1. Materials

The chemical composition of the mild steel (MS) samples utilized in this research was, by weight (in wt%) C: 0.12%, Cr: 0.03%, P: 0.016%, Cu: 0.03%, N: 0.006%, Si: 0.18%, Mn: 0.65%, S: 0.023%, Ni: 0.01%, and Mo: 0.002%, with the balance consisting of iron (Fe). The electrolyte consisted of a 1 M HCl solution, obtained by diluting commercially available 37% hydrochloric acid with bi-distilled water. Inhibitor concentrations varied between 0.1 and 5.0 mM. The aqueous solutions were prepared using bi-distilled water.

All solvents and reagents were obtained from commercial sources Aldrich and Acros and were purchased as analytical grade and used as such. Analytical Thin-Layer Chromatography (TLC) was conducted on E. Merck silica gel 60 F254 precoated plates, with detection carried out under UV light. Melting points were determined on an electrothermal digital melting point apparatus. Nuclear Magnetic Resonance (NMR) (1H$13C)

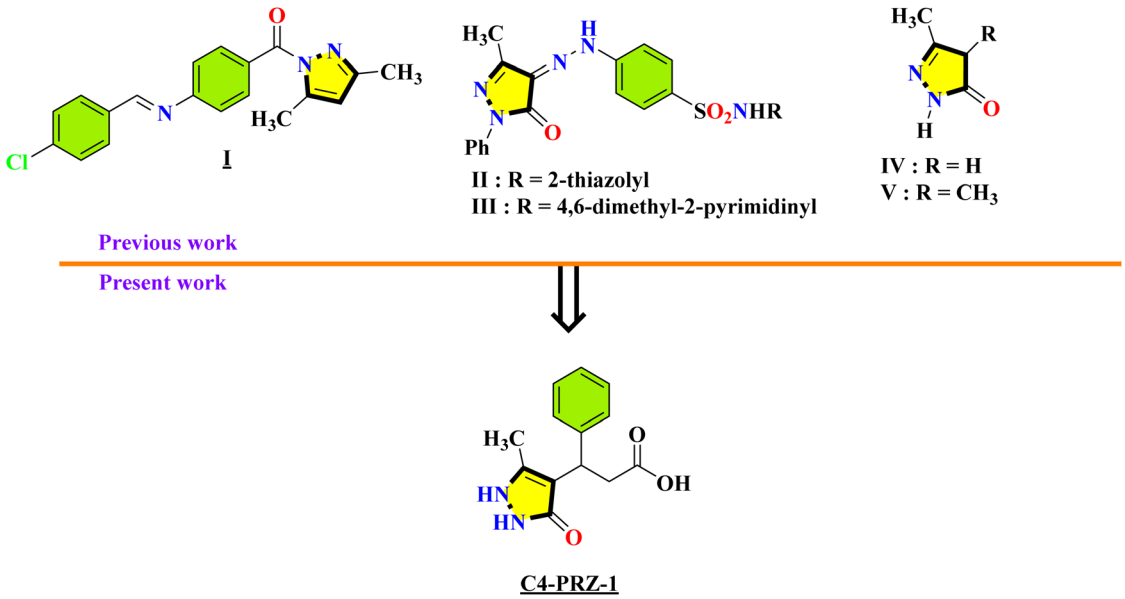

Scheme 1 Pyrazolone derivatives applied as inhibitors against metallic corrosion.

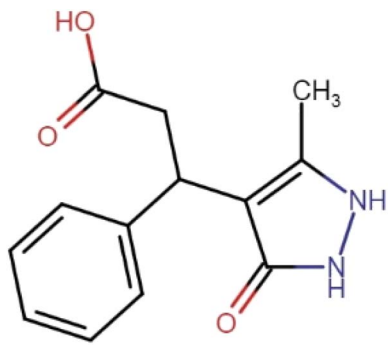

Fig. 1 Molecular structure of C4-PRZ-1.

spectra were recorded in DMSO-d6 ON a JEOL spectrometer with Tetramethylsilane (TMS) as reference.

The inhibitor investigated in this research was (5-methyl-3-oxo-2,3-dihydro-1*H*-pyrazol-4-yl)-3-phenylpropanoic acid, a heterocyclic organic compound referred to as **C4-PRZ-1**, with the molecular formula $C_{13}H_{14}N_2O_3$. The configuration of this compound is illustrated in Fig. 1.

2.2. Synthesis of the inhibitor

We synthesized the β-enaminonitrile intermediate A *via* a multicomponent reaction (MCR) of the cyclocondensation type, involving pyrazolone (78%), benzaldehyde (98,5%), and malononitrile(99%) in absolute ethanol (99,7%), using piperidine (98%) as a base catalyst.[42] The compound 3-(5-methyl-3-oxo-2,3-dihydro-1*H*-pyrazol-4-yl)-3-phenylpropanoic acid (**B**) was then obtained by refluxing the intermediate 6-amino-3-methylpyrano-[2,3-*c*]pyrazole-5-carbonitrile (**A**) with formic acid for 3 hours (Scheme 2).[43] The reaction progress was tracked using thin-layer chromatography (TLC), and upon completion, a single C4-substituted pyrazole product (**B**) was identified. The structures of the produced compounds were validated by ^{1}H and ^{13}C nuclear magnetic resonance (NMR) spectroscopy and with single-crystal X-ray diffraction (SC-XRD) methods.[44,45]

2.2.1 Procedure to prepare compound A. This compound is prepared according to the procedure earlier.[44] To a solution of pyrazolone (4 mmol), benzaldehyde (4 mmol), and malononitrile (4 mmol, 260 mg) in 15 mL of absolute ethanol, two drops of piperidine were added. The reaction mixture was refluxed under magnetic stirring for 30 min. The progress of the reaction was monitored by thin-layer chromatography (TLC) using a methanol/chloroform mixture as the eluent. After cooling to room temperature, the resulting precipitate was filtered and recrystallized from ethanol to afford compound **A** in 95% yield.

2.2.2 Procedure to prepare compound C4-PRZ-1. This compound is prepared according to the procedure earlier.[45] Compound **A** was added to 5.0 mL of formic acid, and the reaction

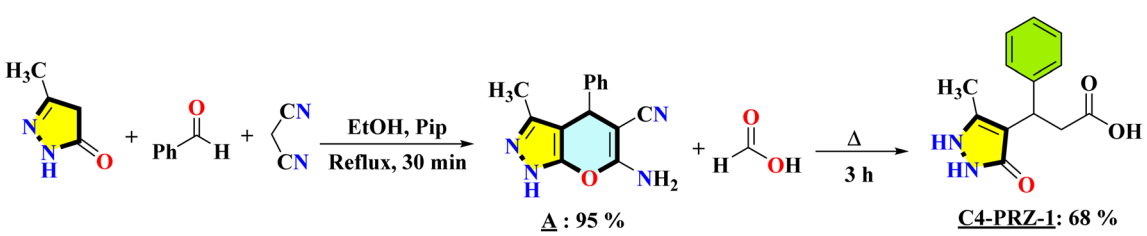

Scheme 2 Synthesis of dihydropyrano[2,3-*c*]pyrazole compounds A and pyrazolone B.

mixture was refluxed under magnetic stirring for 3 hours. After completion, the reaction mixture was poured onto 5.0 g of ice. The resulting precipitate was collected by filtration and recrystallized from ethanol to afford compound **C4-PRZ-1** in 68% yield.

2.3. Electrochemical measurements

The potentiodynamic polarization (PDP) tests carried out after immersion about 1 hour (since we began by OCP for 30 min then at least 20 min of EIS), the potential was swept from −800 mV to 0 mV at a scan rate of 1 mV s^{-1}, with all potential values referenced to the saturated calomel electrode (SCE). EIS measurements were carried out at the open-circuit potential (OCP) following 30 minutes of immersion. The frequency range for EIS started at 100 000 Hz and decreased to 0.010 Hz, with an AC sinusoidal signal amplitude of 10 mV. For the electrochemical experiments carried out with PGZ 100 ALL-IN-ONE Volta Lab potentiostat controlled by a computer *via* Voltamaster software equipped with an electrochemical cell with three-electrode: the working electrode (WE) consisted of a MS disk with a diameter of 1 cm and an exposed surface area of 0.785 cm^2. A platinum plate with a surface area of 1 cm^2 functioned as the counter electrode (CE), whereas a saturated calomel electrode (SCE) was employed as the reference electrode. Before immersion in the acid solution, the working electrode (WE) was polished with emery paper up to 1200 grit, thoroughly rinsed with distilled water, and then cleaned using acetone. Each experiment was conducted thrice to ensure precision.

The inhibition efficiency (η%) of the inhibitor was determined using the corrosion current density obtained from the PDP data and the charge transfer resistance derived from the EIS results, based on the following equations:

$$\eta_p(\%) = \frac{i_o - i_{inh}}{i_o} \times 100 \quad (1)$$

where i_o and i_{inh} represent the corrosion current densities without and with the inhibitor, respectively.

$$\eta_{EIS}(\%) = \frac{R_{inh} - R_o}{R_{inh}} \times 100 \quad (2)$$

where R_{inh} and R_o represent the values of the charge transfer (polarization) resistance of the MS electrode with and without the addition of the inhibitor (**C4-PRZ-1**), respectively.

The extent of surface covering for various concentrations of the C4-substituted pyrazolone was determined using the subsequent equation:

$$\text{Surface coverage } (\theta) = (i_o - i_{inh})/i_o \quad (3)$$

where i_o and i_{inh} denote the corrosion current densities measured in the absence and presence of the corrosion inhibitor **C4-PRZ-1**, respectively, calculated by the intersection of the extrapolated Tafel lines at the corrosion potential for MS in both uninhibited and inhibited acidic environments.

2.4. Surface analytical techniques

The samples (a), (b) and (c) for SEM-EDS measurements were polished using emery papers with grits ranging from 100 to 1200, followed by degreasing with acetone and drying. Morphological images were obtained from three different sets of samples: (a) dry, polished samples that were not exposed to any solution, (b) samples that were immersed for 24 hours in a blank 1 M hydrochloric acid solution, and (c) samples immersed in 1 M HCl for 24 hours in the presence of an inhibitor at a concentration of 1.0 mM. The morphology and microstructure were examined using SEM (Supra 40 VP Gemini, Zeiss, operating at a maximum voltage of 20 kV), while the elemental composition was analyzed by obtaining energy dispersive X-ray (EDX) spectroscopy.

2.5. DFT and Monte Carlo simulation details

Recently, Density Functional Theory (DFT) has become a powerful quantum chemical computational method widely employed to study the electronic and structural effects influencing the anti-corrosive properties of inhibitors on metals.[46] The molecular geometries were optimized using the GGA/BLYP approach with a DNP 3.5 basis set in an aqueous environment, applying the COSMO solvation model with water as the solvent. All computations were carried out with the DMol3 software package. After optimizing the structures, several key reactivity indicators were calculated as detailed in previous literature.[42,43]

Monte Carlo simulations, coupled with a simulated annealing algorithm (MCS-SAA) and utilizing an adsorption locator tool, were achieved to examine the interfacial interactions between the inhibitor and the Fe (110) surface.[47] The simulation consisted of three cycles, with each cycle containing 15 000 steps and employing the COMPASS force field. The simulations were carried out under periodic boundary conditions, utilizing a box that included a metal slab made up of 8 × 8 Fe atoms and an upper aqueous layer measuring 50 Å, which contained a single **C4-PRZ-1** molecule. The Ewald summation method was used to determine electrostatic interactions, whereas van der Waals interactions were assessed through atom-based summation.

2.6. Toxicological safety and environmental impact prediction

The designed C4-substituted heterocyclic pyrazolone was evaluated using computational tools to assess both its toxicological safety and environmental impact, as these factors are crucial for its potential application as a corrosion inhibitor. The ProTox-III, and ECOSAR online softwares are used. Pro Tox-III predicts the Toxicity endpoints in human and for environmental also in terms of Ecotoxicity. ECOSAR is a free software program developed by United States Environmental Protection Agency, that estimates the acute and chronic toxicity of organic chemicals to aquatic organisms based on their structure and properties.[35]

3. Results and discussion

3.1. Electrochemical measurements

3.1.1 Potentiodynamic polarization experiments

3.1.1.1 Effect of the inhibitor concentration. Polarization curves for mild steel (MS) were measured in a 1 M HCl solution

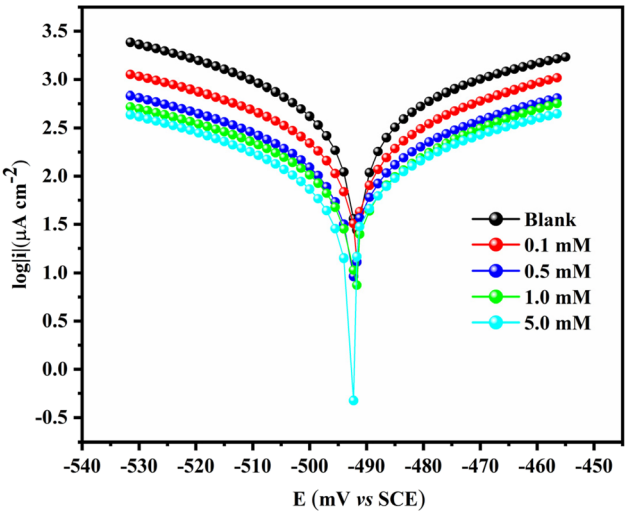

Fig. 2 Polarization curves for mild steel in 1 M HCl at varying concentrations of C4-PRZ-1 at 298 K.

in the presence and absence of the inhibitor, exhibiting typical Tafel behavior. Fig. 2 illustrates the Tafel plots for various concentrations of **C4-PRZ-1** in a 1 M HCl solution at 298 K. The electrochemical characteristics, like corrosion potential (Ecorr *versus* SCE), corrosion current density (i_{cor}), surface coverage (θ), inhibition efficiency (η%), and cathodic and anodic Tafel slopes (β_a, β_c) were determined from these plots, and are shown in Table 1. The surface coverage values for various inhibitor concentrations were determined using eqn (3).

Fig. 2 shows that the addition of the **C4-PRZ-1** inhibitor notably reduces the corrosion rate, evidenced by the shift of both anodic and cathodic polarization curves to lower current densities. This decrease is due to a reduction in the rates of anodic metal dissolution and cathodic hydrogen evolution reactions, which become more pronounced as the inhibitor concentration increases. This behavior indicates that **C4-PRZ-1** functions as mixed inhibitor, reducing the corrosion of mild steel in a 1 M hydrochloric acid solution by covering active sites on the metal surface and establishing a protective barrier against the acidic medium. Notably, the cathodic Tafel curves illustrate that the inhibitor has no significant impact on the reduction of hydrogen ions, suggesting that hydrogen evolution on the MS surface primarily proceeds through a charge transfer mechanism. This pattern was observed consistently across all the evaluated inhibitors.[48]

The data shown in Table 1 demonstrate that an increase in the concentration of **C4-PRZ-1** correlates with improvements in both inhibition efficiency and corrosion current density. This effect may be ascribed to the development of an adsorbed inhibitor layer on the metal surface. The presence of the inhibitor caused a smaller negative shift in the corrosion potential (E_{corr}), while the cathodic and anodic Tafel slopes (β_c and β_a) remained largely unchanged. This suggests that **C4-PRZ-1** acts as a mixed-type corrosion inhibitor.[49]

3.1.1.2 Effect of temperature on the inhibition efficiency. Temperature significantly influences the rate of corrosion and the effectiveness of inhibitors. The influence of temperature on the corrosion characteristics of MS in a 1 M HCl solution, both with and without the inclusion of 1.0 mM **C4-PRZ-1**, was assessed at four distinct temperatures: 298, 308, 318, and 328 K.

The effect of temperature provides valuable insight into the adsorption behavior and inhibitory performance of the compound at elevated temperatures. To this end, the inhibition efficiency of the **C4-PRZ-1** molecule was evaluated in a corrosive medium using the potentiodynamic polarization technique over the temperature range of 298–328 K, at a fixed concentration of 1 mM. The corresponding Tafel polarization curves are illustrated in Fig. 3 and 4, and the derived electrochemical parameters are summarized in Table 2.

In the absence of the inhibitor (blank HCl solution), a noticeable increase in the corrosion current density (i_{corr}) was

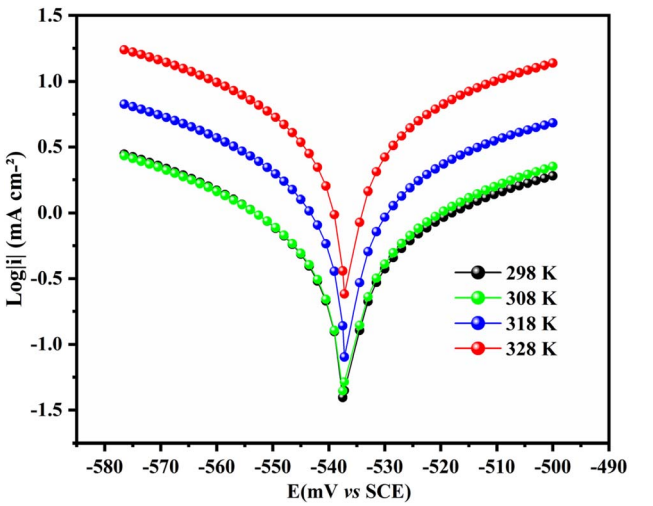

Fig. 3 Polarization curves for MS in 1 M HCl blank solution at different temperatures.

Table 1 Potentiodynamic polarization data for MS in 1 M HCl, both in the absence and presence of varying amounts of the inhibitor (C4-PRZ-1) at 298 K

C4-PRZ-1 C_{inh} (mM)	β_a (mV dec^{-1})	β_c (mV dec^{-1})	R_p (Ω cm^2)	i_{cor} (μA cm^{-2})	E_{corr} (mV/SCE)	Surface coverage (θ)	η_p (%)
0.0	63.4	−57.3	17.86	558.4	−491.62	—	—
0.1	66.1	−68.0	39.23	290.8	−491.03	0.48	48
0.5	53.5	−54.5	64.22	138.4	−491.02	0.75	75
1.0	56.1	−64.2	81.04	127.9	−491.00	0.77	77
5.0	59.8	−63.4	105.35	82.8	−491.20	0.85	85

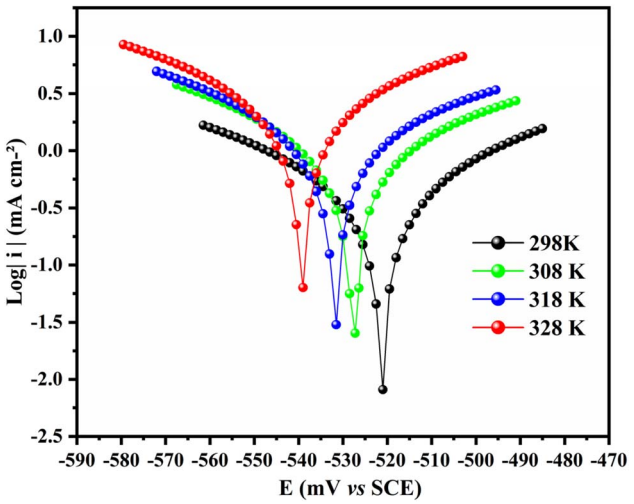

Fig. 4 Polarization curves for MS in 1 M HCl containing 1 mM C4-PRZ-1 at various temperatures.

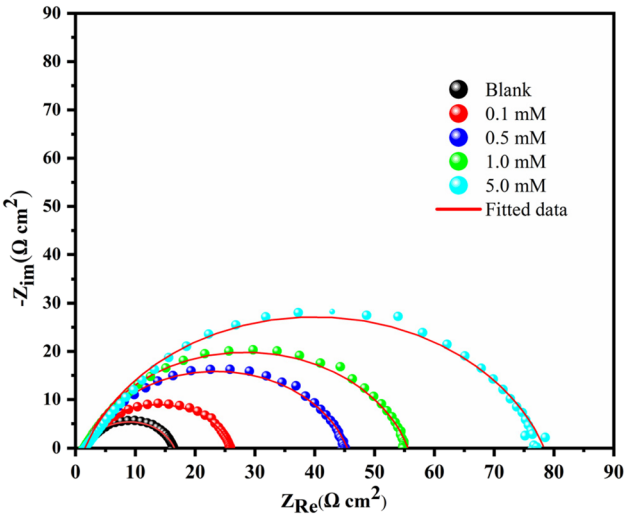

Fig. 5 Nyquist impedance graphs for MS in 1 M HCl solution with varying concentrations of C4-PRZ-1 at 298 K.

observed with rising temperature, indicating an acceleration of the corrosion process. Conversely, the introduction of **C4-PRZ-1** resulted in a marked reduction in i_{corr} values across all studied temperatures, signifying its inhibitory action. However, the inhibition efficiency (IE%) determined by the PDP method was found to be temperature-dependent. Specifically, increasing the temperature led to an enhancement in IE%, which reached 95% at 328 K. This is presumably due to an increase in adsorption of the inhibitor as reported elsewhere.[50–52]

3.1.2 EIS measurements

3.1.2.1 Effect of the inhibitor concentration. To enhance understanding of the inhibitory mechanism and corroborate findings from polarization studies, Electrochemical Impedance Spectroscopy (EIS) was performed, which is a robust alternating current (AC) technique for analyzing corrosion processes. The impedance response of MS, under both conditions of changing concentrations of **C4-PRZ-1** and its absence, is depicted through Nyquist and Bode plots presented in Fig. 5 and 6.

Initially, the Nyquist plot for the blank solution showed a well-defined peak indicating a characteristic relaxation time. Upon adding **C4-PRZ-1**, changes appeared in the semicircles of the Nyquist plots, suggesting surface irregularities and non-uniform electrode characteristics due to the inhibitor's adsorption (Fig. 5). These alterations are linked to frequency dispersion, which is typical of an inhomogeneous electrode surface.[53]

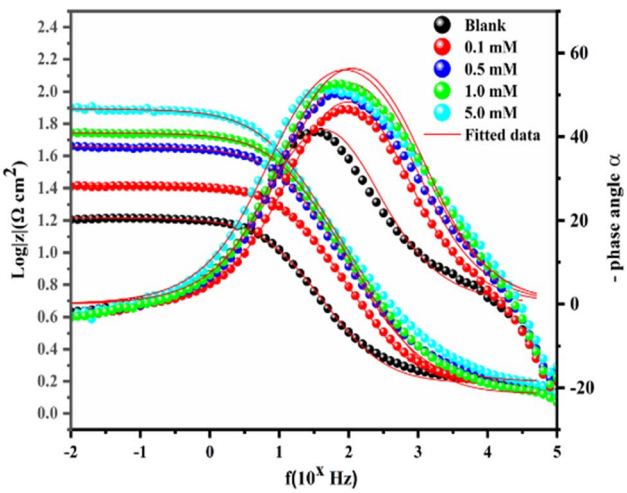

Fig. 6 Bode and phase angle graphs of MS in 1 M HCl solution, both in the absence and in presence of varying amounts of C4-PRZ-1 at 298 K.

When comparing the effects of inhibitor concentrations, the Nyquist plots revealed two distinct regions after introducing **C4-PRZ-1**. The high-frequency (HF) region presented a semicircle; indicative of a capacitive loop associated with double-layer

Table 2 Impact of temperature on the electrochemical characteristics with and without the C4-PRZ-1 inhibitor

	T (K)	E_{corr} (mV/SCE)	i_{cor} (μA cm^{-2})	β_c (mV dec^{-1})	β_a (mV dec^{-1})	η_p (%)
	298	−537.50	554.0	−55.0	58.3	—
Blank	308	−537.50	636.0	−60.6	76.9	—
	318	−537.32	1512.0	−59.3	70.9	—
	328	−537.13	4642.0	−68.3	77.0	—
C4-PRZ-1	298	−521.00	80.9	−68.2	65.5	85.39
Added	308	−527.23	82.8	−57.1	68.3	86.98
	318	−531.50	134.0	−70.9	91.3	91.13
	328	−539.00	203.1	−62.7	69.3	95.62

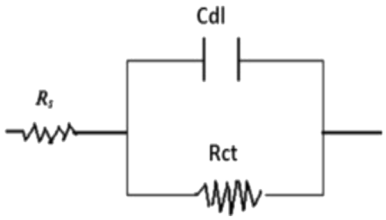

Fig. 7 The equivalent electrical circuit proposed for the experimental impedance data.

capacitance (C_{dl}) and charge transfer resistance (R_{ct}). Meanwhile, in the low-frequency (LF) region, a linear plateau emerged, corresponding to a diffusion-controlled process within the electrolyte.[54] The two observed capacitive loops, whose dimensions increased with higher inhibitor concentrations, highlighted the strong dependence of **C4-PRZ-1**'s inhibitory performance on its concentration. The HF loop relates to the charge transfer process, while the LF loop corresponds to the development of an oxide layer on the MS surface.

The system's equivalent circuit model, shown in Fig. 7, includes three key components: double-layer capacitance (C_{dl}), charge-transfer resistance (R_{ct}), and solution resistance (R_s). These components were extracted from the Nyquist data. The presence of depressed semicircles in the Nyquist plots is ascribed to reasons like impurities, surface roughness, and variations in the distribution of active sites. In all Nyquist plots, a single capacitive loop with a suppressed semicircular shape was consistently observed, suggesting a dominant charge transfer mechanism during the corrosion process.[44] The corresponding Bode plots also displayed a single time constant, further supporting this observation (Fig. 6).

The single capacitive loop indicates that the charge transfer process is the primary mechanism governing the corrosion behavior. Interestingly, the addition of **C4-PRZ-1** did not significantly alter the configuration of the Nyquist plots, suggesting that the inhibitor does not modify the fundamental corrosion mechanism but rather decreases the corrosion rate through a surface-blocking effect.

To enhance the accuracy of the impedance analysis, a constant phase element (Q) was incorporated into the equivalent circuit model, as shown in Fig. 7. The double-layer capacitance (C_{dl}) at various concentrations of **C4-PRZ-1** was computed using the subsequent equation:[32]

$$C_{dl} = (Q \times R_{ct}^{1-\Phi})^{1/\Phi} \quad (5)$$

where Q represents the constant phase element and Φ denotes the phase shift.

Table 3 displays the C_{dl} values, the R_{ct} values obtained from the Nyquist diagram, and the corresponding η_{EIS} (%) values calculated based on these data.

As shown in Table 3, the addition of the inhibitor (**C4-PRZ-1**) leads to a reduction in C_{dl} relative to the blank solution. This

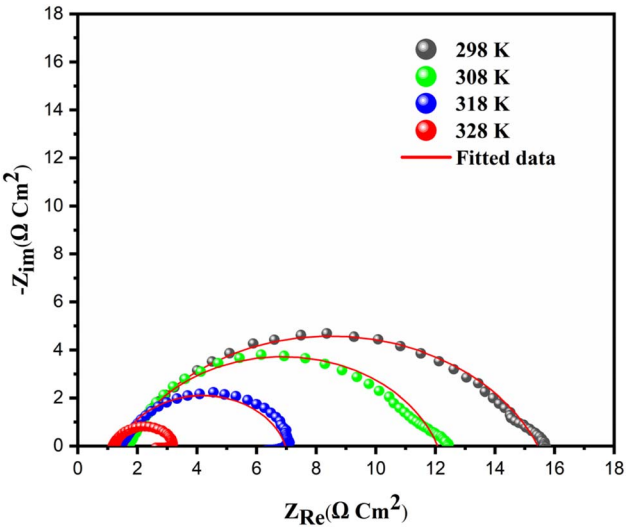

Fig. 8 Nyquist impedance diagrams for MS in a 1 M HCl blank solution at various temperatures.

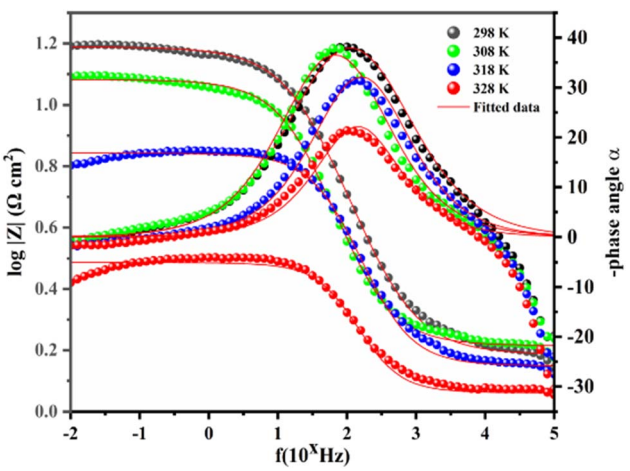

Fig. 9 Bode and phase angle graphs of MS in 1 M HCl blank solution at various temperatures.

Table 3 EIS characteristics obtained from the impedance spectra of MS with and without inhibitor (**C4-PRZ-1**) at 298 K

C4-PRZ-1 C_{inh} (mM)	R_{ct} (Ω cm^2)	R_s (Ω cm^2)	Φ	$Q \times 10^{-3}$ (s^n Ω cm^{-2})	C_{dl} (μF cm^{-2})	η_{EIS} (%)	θ ($\pm 10^{-2}$)	χ^2
0.0	15.00	1.526	0.7893	2.6370	1113.369	—	—	0.051
5.0	76.80	1.574	0.784	0.6533	286.470	80	0.80	0.096
1.0	54.28	1.320	0.8035	0.6176	269.199	72	0.72	0.087
0.5	43.91	1.540	0.7961	0.7310	302.964	65	0.65	0.070
0.1	24.57	1.485	0.8034	0.9836	395.527	39	0.39	0.058

suggests that the inhibitor adsorbs onto the MS surface. Additionally, the R_{ct} increases in the presence of the inhibitor, demonstrating its ability in diminishing the dissolution rate of MS in 1 M HCl. The highest η% value, approximately 80%, was achieved at a **C4-PRZ-1** concentration of 5 mM. There are slight variations in inhibition efficiency values obtained using EIS and direct current PDP methods at different concentrations, indicating a satisfactory correlation between these electrochemical techniques.

3.1.2.2 Effect of temperature on the inhibition efficiency. Fig. 8–11 illustrate the effect of temperature, presenting Nyquist, Bode, and phase angle graphs for MS immersed in 1 M HCl at different temperatures (298, 308, 318, and 328 K), both with and without the presence of **C4-PRZ-1**. The depressed semicircles observed in the Nyquist plots indicate surface heterogeneity, impurities, and a non-uniform distribution of active sites.[55–57]

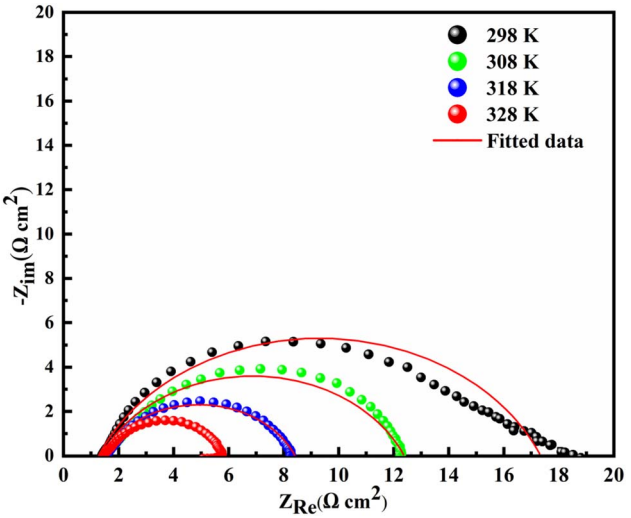

Fig. 10 Nyquist impedance graphs for MS in 1 M HCl solution containing 1 mM of inhibitor (C4-PRZ-1) at various temperatures.

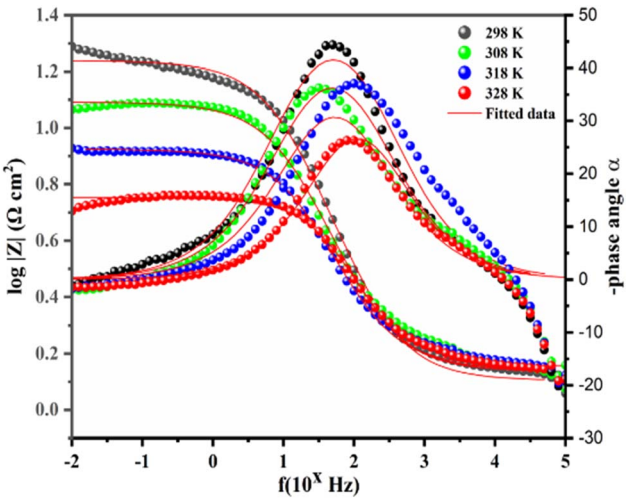

Fig. 11 Bode plots of MS in 1 M HCl solution in the presence of 1 mM inhibitor (C4-PRZ-1) at different temperatures.

Each plot features a single capacitive loop resembling a depressed semicircle, indicative of a unique time constant in the Bode representations, implying that the dominant electrochemical mechanism is charge transfer.[58,59] The Nyquist plots remain unchanged after the addition of **C4-PRZ-1** at a concentration of 1 mM across all temperatures, suggesting that the inhibitor does not alter the corrosion mechanism but functions by a simple blocking effect, thus reducing the corrosion rate.[60]

The Bode plots (Fig. 9 and 11) reveal a noticeable shift in phase angle (Φ) as the temperature increases, which can be attributed to changes in the metal-solution interface. This shift is primarily attributed to the generation of a protective film on the MS surface, which modifies the microstructural properties.[61]

3.2. Adsorption isotherms

The R^2 correlation coefficient was employed to ascertain the most suitable adsorption isotherm this study. The analysis indicated that the Langmuir isotherm (eqn (6)) provided the best fit, as illustrated in Fig. 12, with an R^2 value nearing unity. These findings indicate that the adsorption behavior of the **C4-PRZ-1** inhibitor on the mild steel surface in a 1 M HCl solution conforms to the Langmuir adsorption model. The Langmuir model presumes a uniform metal surface with a fixed number of adsorption sites, where all sites are equivalent, and each site can accommodate only a single adsorbate molecule. Additionally, it assumes no lateral interactions between molecules adsorbed on the surface.[62]

$$\frac{C_{inh}}{\theta} = \frac{1}{K_{ads}} + C_{inh} \quad (6)$$

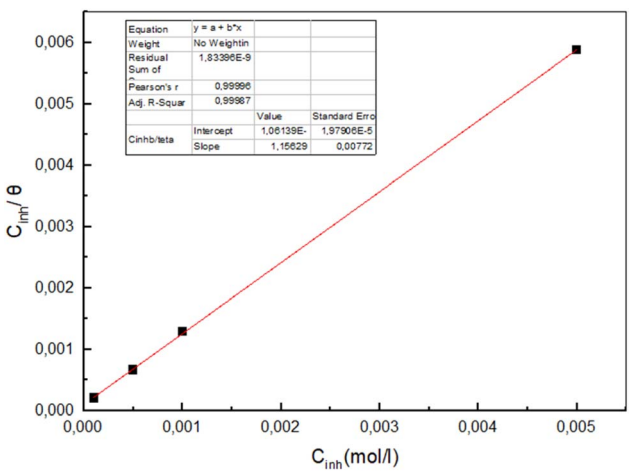

Fig. 12 Langmuir adsorption isotherm of C4-PRZ-1 on MS surface at 298 K.

Table 4 Parameters of linear regression derived from the fitted line of Fig. 12

Inhibitor	Slope	K_{ads} (L mol^{-1}) $\times 10^4$	R^2	ΔG°_{ads} (KJ mol^{-1})
C4-PRZ-1	1.1563	0.9421	0.999	−32.6

Fig. 12 shows a straight line of $\frac{C_{inh}}{\theta}$ *versus* C_{inh}, where C_{inh} represents the inhibitor (**C4-PRZ-1**) concentration, K_{ads} denotes the adsorption equilibrium constant, and θ signifies the surface coverage area.

The standard Gibbs free energy of adsorption, ΔG°_{ads}, is connected to the adsorption constant K_{ads} through eqn (7):

$$\Delta G^{\circ}_{ads} = -RT\ln(55.5K_{ads}) \quad (7)$$

where 55.5 represents the molar concentration of water in the solution. The values for K_{ads} and ΔG°_{ads} are presented in Table 4. A negative ΔG°_{ads} value signifies that the adsorption process is spontaneous, suggesting the formation of a stable protective

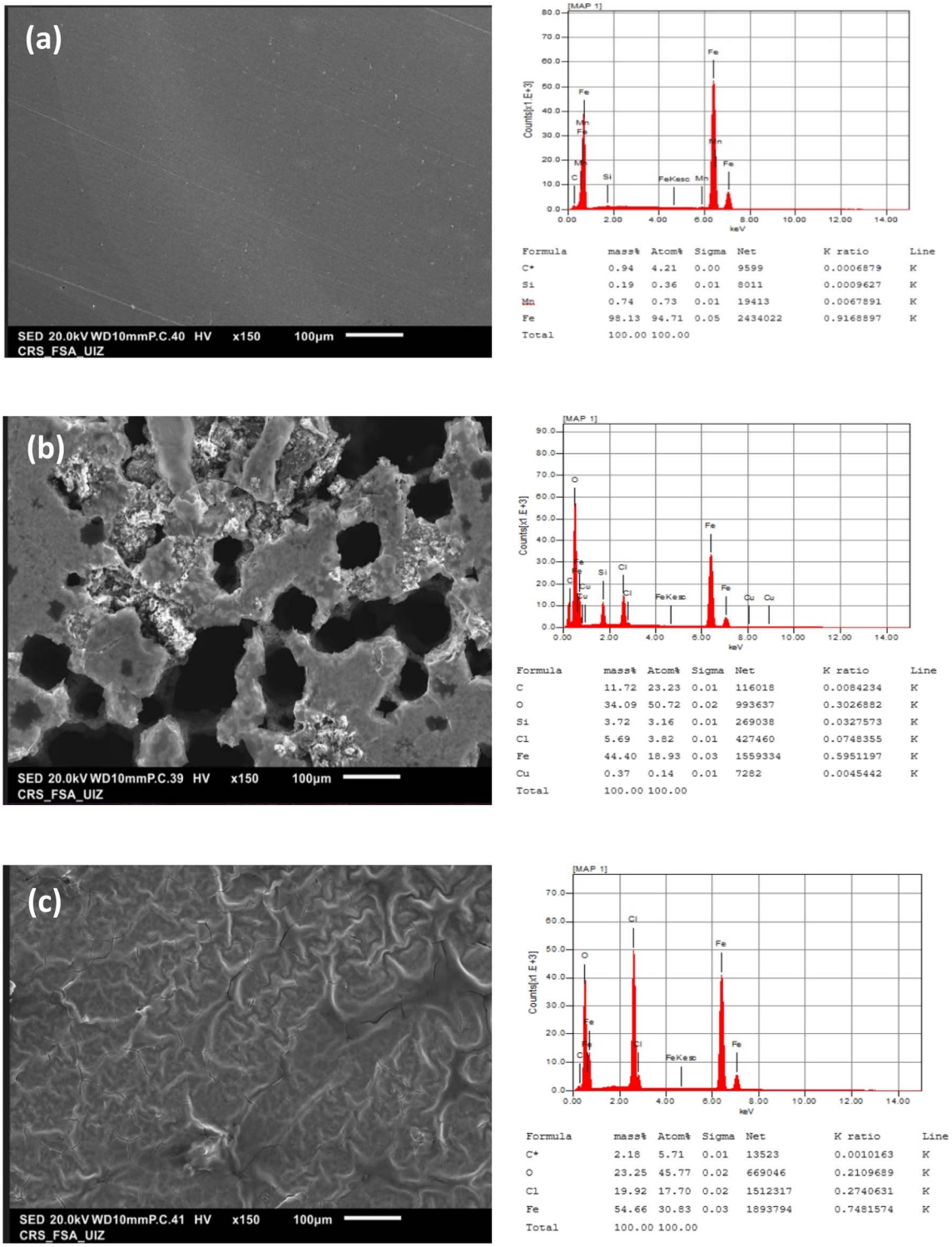

Fig. 13 SEM images and EDS compositional results for (a) the MS specimen alone, (b) after 24 h of immersion time without inhibitor, and (c) immersion with 1 mM **C4-PRZ-1**.

film on the steel surface.[63] Literature indicates that ΔG°_{ads} values of $\leq$ 20 kJ mol^{-1} are typical of physisorption, while values $\geq$ 40 kJ mol^{-1} are indicative of chemisorption, involving charge transfer or sharing between the inhibitor and the metal surface.[64] In this research, the calculated ΔG°_{ads} value suggests that the **C4-PRZ-1** inhibitor is adsorbed onto the mild steel surface through mixed adsorption mechanism, incorporating both physical and chemical interactions, with a predominance of chemisorption. It is plausible that the adsorption initially occurs through electrostatic attraction between the inhibitor and the metal surface (physisorption), followed by the establishment of stronger chemical bonds (chemisorption) as the inhibitor molecules anchor more firmly onto the surface.[64]

3.3. Surface morphology analysis results

Fig. 13a–c present the SEM images and EDS analysis of mild steel (MS) samples following 24 hours of immersion in 1 M HCl, with and without the presence of 1 mM **C4-PRZ-1** at 298 K. The EDS analysis, performed over the entire exposed surface (Fig. 13a), reveals that in the absence of the inhibitor (Fig. 13b), the surface composition is predominantly iron, along with a substantial chlorine (Cl^-) peak. However, in the presence of **C4-PRZ-1** (Fig. 13c), the surface shows significantly less damage and a reduced Cl^- peak. The elevated carbon (C) content confirms the adsorption of **C4-PRZ-1** on the MS surface, indicating the presence of the inhibitor film.

The SEM micrograph in Fig. 13a, representing the pre-immersion condition, reveals a smooth and uniform metal surface, with visible polishing marks. Fig. 13b illustrates the MS surface subjected to 1 M HCl for 24 hours without the inhibitor, displaying extensive corrosion characterized by deep pits, cracks, and a porous structure, which are indicative of severe degradation by the acidic medium. In contrast, Fig. 13c, corresponding to the inhibited sample, shows a notably smoother and less deteriorated surface, suggesting the establishment of a protective inhibitor layer. This thin film acts as a temporary barrier, shielding the metal from direct acid exposure and significantly mitigating the overall corrosion rate.

3.4. DFT calculations

Determining the electronic parameters of a molecule is a powerful approach to understanding and predicting its reactivity in various chemical reactions. This methodology is particularly valuable in the design and optimization of corrosion inhibitors, as it enables researchers to forecast their performance and interaction mechanisms, leading to the creation of more effective inhibitory compounds. One of the key theoretical frameworks used for this purpose is the Frontier Molecular Orbital (FMO) theory, which helps identify potential adsorption centers of an inhibitor molecule when it interacts with Fe atoms on a metal surface.

The Highest Occupied Molecular Orbital (HOMO) represents the orbital with the highest energy that contains electrons, and it plays a critical role in chemical processes involving electron donation. Conversely, the Lowest Unoccupied Molecular Orbital (LUMO) corresponds to the orbital with the lowest energy that is unoccupied by electrons and is primarily involved in electron-accepting processes. In Fig. 14, the spatial distribution of the frontier molecular orbitals for the investigated inhibitor is illustrated. The LUMO is predominantly localized on the pyrazole ring and the central –COOH group, indicating these regions as potential sites for electron acceptance. In contrast, the HOMO is predominantly situated on the pyrazole ring, suggesting it is the primary site for electron donation.

For further insight into the electrostatic interactions between the metal surface and the inhibitor molecule, Electrostatic Potential (ESP) maps can be employed. Fig. 14 illustrates the ESP map of the analyzed inhibitor, employing color coding to depict varying charge distributions: red regions signify electron-rich places (negative potential), whereas blue regions represent electron-deficient areas (positive potential). The red regions, predominantly associated with N and O atoms, are likely to interact with the electropositive metal surface during the initial stages of the adsorption process.[65–68]

Additionally, Fukui functions were applied to assess both local and global reactivity characteristics of the inhibitor molecule concerning its interaction with the MS surface. This analysis allows the identification of electrophilic and nucleophilic sites within the molecule, providing a deeper understanding of the specific interaction sites that are most favorable for binding to the metal surface.

$$\text{For the nucleophilic attack: } f_k^+ = q_{N+1} - q_N \quad (8)$$

$$\text{For the electrophilic attack: } f_k^- = q_N - q_{N-1} \quad (9)$$

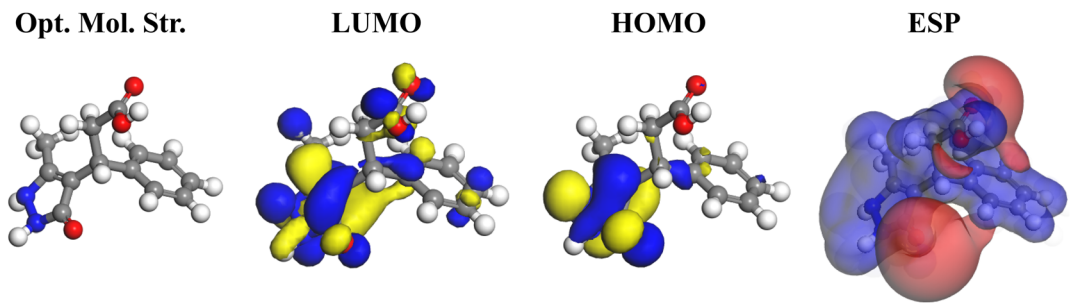

Fig. 14 Optimized molecular configuration, frontier molecular orbital distribution (*i.e.*, HOMO and LUMO), and ESP map of the **C4-PRZ-1** inhibitor.

The values of these Fukui functions were used to examine which atoms in the inhibitors were more prone to undergo electrophilic or nucleophilic attack.

As shown by eqn (8) and (9), the f_k^- function represents the reactivity related to the electrophilic attack, or when the molecule loses electrons, and the f_k^+ function corresponds to the reactivity to nucleophilic attack and refers to the change in density when an organic molecule gains an electron.

Table 5 illustrates that the sites at which the studied inhibitor acted as favorable centers for nucleophilic attack were the C13, C16, and O18 atoms, which are located on the pyrazole ring. However, C8, N14. The N15 and O16 atoms are more suitable for electrophilic attack.

The neutral Pyrazolone molecule, with a high EHOMO (−5.039 eV) and low ELUMO (−1.258 eV), demonstrates a strong ability to both donate and accept electrons. The energy gap (ΔE) is a critical factor that reflects the reactivity of organic molecules toward a protected metal surface.[69] A smaller ΔE signifies higher molecular reactivity and increased polarizability, which enhances the molecule's adsorption onto the metal surface.[70] In the case of **C4-PRZ-1**, as outlined in Table 6, its low ΔE value (3.781 eV) contributes to its robust adsorption on the MS surface, thereby forming a stable protective barrier against corrosion.

Table 5 Fukui indices for electrophilic (f_k^-) and nucleophilic (f_k^+) attack by the inhibitor

Atom	f_k^+	f_k^-
C (1)	0.023	0.004
C (2)	−0.003	−0.003
C (3)	0.009	0.009
C (4)	0.018	0.009
C (5)	0.023	0.013
C (6)	0.009	0.008
C (7)	−0.014	−0.021
C (8)	0.033	0.099
C (9)	−0.006	−0.008
C (10)	0.054	0.005
O (11)	0.061	0.015
O (12)	0.029	0.004
C (13)	0.116	0.052
N (14)	0.05	0.144
N (15)	0.048	0.078
C (16)	0.076	0.062
C (17)	−0.013	−0.003
O (18)	0.091	0.196

Table 6 Quantum chemical characteristics of C4-PRZ-1

E_{HOMO}	E_{LUMO}	ΔE	η	X	$\Delta N_{Fe(110)}$
(eV)	(eV)	(eV)	(eV)	(eV)	(e)
−5.039	−1.258	3.781	1.891	3.148	0.442

The electron transfer from the inhibitor to vacant sites on the metal surface (in this case, Fe (110)) is measured by the ΔNFe(110) parameter. A positive ΔN value indicates electron donation to the metal. Table 6 indicates that the ΔN value of 0.442 *e* implies that **C4-PRZ-1** promotes a modest electron transfer to the metal surface, potentially aiding in the development of a protective layer that safeguards the metal from corrosion.[71]

3.5. Monte Carlo simulations

Monte Carlo simulation (MCS) was conducted to model the mechanism of inhibitor adsorption on the iron surface. Fig. 15 displays the most stable conformation of the **C4-PRZ-1** molecule on the Fe (110) surface as determined by the MCS. The inhibitor molecule aligns horizontally and parallel to the target metal surface, which maximizes the contact and increases the surface coverage. Such an orientation results in higher adsorption energy and reflects the greater inhibition efficiency of the investigated inhibitor.

In contrast, the adsorption energy of the inhibitor molecule on the Fe (110) surface under solvation conditions was calculated to be −86.178 kJ mol^{-1}. The negative adsorption energy indicates that the inhibitor can spontaneously interact with the metal surface atoms and competitively adsorb onto the surface. This interaction promotes the generation of a stable, protective layer on the metal surface.[72]

3.6. Hypothetical inhibition mechanism

Experimental results indicate that organic compounds containing heteroatoms such as oxygen, nitrogen, or sulfur exhibit significant corrosion inhibition properties, primarily due to their ability to coordinate with the metal surface through lone pair electron donation.[4] The observed inhibition performance of **C4-PRZ-1** is closely associated with its adsorption at the steel/electrolyte interface,[73,74] as supported by electrochemical and surface characterization techniques. The electrochemical measurements indicate that **C4-PRZ-1** functions as mixed-type

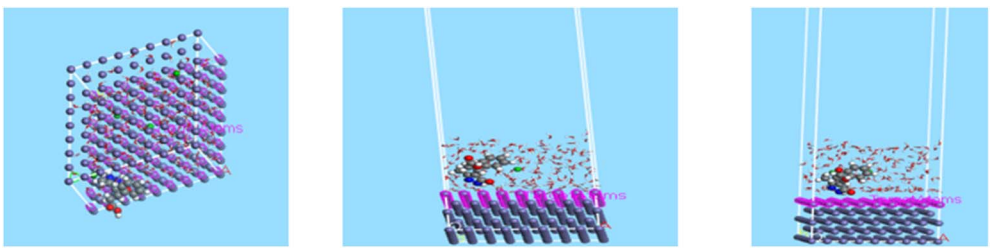

Fig. 15 Equilibrium adsorption configuration of the tested inhibitor on the Fe (110) surface.

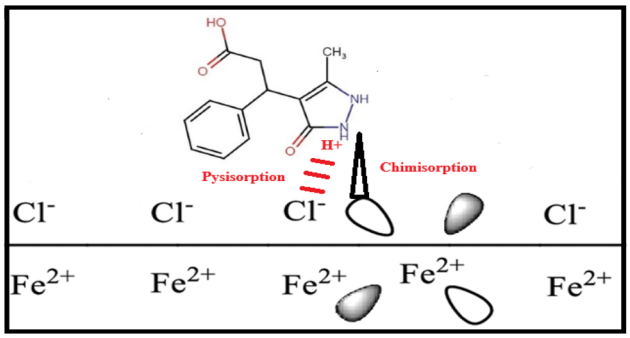

Fig. 16 Mechanistic diagram of the adsorption of the inhibitor (C4-PRZ-1) on the MS surface.

inhibitor and operates through a single charge transfer mechanism at the metal-electrolyte interface. This is consistent with the recorded shift in corrosion potential and changes in Tafel slope values. The inhibition efficiency is largely explained by a strong physisorption-driven mechanism, as inferred from the adsorption behavior and supported by the conformity to the Langmuir isotherm model. The adsorption mechanism involves both physisorption and chemisorption processes, driven by electrostatic interactions between the charged metal surface and the inhibitor molecules. Additionally, electron pair donation from the inhibitor to the vacant d-orbitals of the steel surface contributes to the overall adsorption orbitals (Fig. 16). Surface analysis and theoretical modeling suggest that, under acidic conditions, the mild steel surface becomes positively charged,[75] promoting the adsorption of chloride ions (Cl^-) and creating a locally negative environment.[76–78] This environment facilitates for **C4-PRZ-1** molecule, the formation of a protective layer that hinders further corrosion. Therefore, the experimentally supported inhibition mechanism of **C4-PRZ-1** involves adsorption onto the mild steel surface through both electrostatic interactions and electron pair donation of inhibitor, predominantly affecting the mixed processes, and resulting in effective corrosion mitigation.

3.7. Toxicity and environmental impact

The designed C4-substituted heterocyclic pyrazolone was evaluated using computational tools to assess both its toxicological safety and environmental impact, as these factors are crucial for its potential application as a corrosion inhibitor.

3.7.1 Toxicity assessment. Using ProTox-III, the compound was predicted to be inactive for carcinogenicity, immunotoxicity, mutagenicity, cytotoxicity, ecotoxicity, and nutrient toxicity, with corresponding probabilities of 0.53, 0.99, 0.67, 0.74, 0.81, and 0.61, respectively. These predictions suggest that the molecule is unlikely to exert adverse effects on human health. The high confidence levels for immunotoxicity (0.99) and ecotoxicity (0.81) further support a low toxicity profile, indicating that the compound is not expected to pose major risks to non-target species in the environment.[44]

3.7.2 Ecotoxicity and environmental relevance. Ecotoxicity refers to the potential harmful effects of chemicals on aquatic and terrestrial organisms, including fish, algae, daphnia, soil microorganisms, and plants. The *in silico* ecotoxicity prediction (ProTox-III, probability 0.81) classified the compound as inactive, suggesting it does not pose acute toxicity risks to environmental organisms. This is particularly important because corrosion inhibitors often find their way into industrial effluents and may reach water bodies. Ecotoxicity is not limited to acute lethality; long-term effects such as bioaccumulation, disruption of microbial communities, or chronic impacts on aquatic life must also be considered. Given the aromatic and moderately polar nature of the pyrazolone scaffold, persistence in aquatic systems cannot be excluded.[34,37] Thus, although acute ecotoxicity is predicted to be minimal, the possibility of chronic sublethal effects warrants future experimental validation.

3.7.3 Biodegradation and environmental fate. QSAR-based biodegradation modeling provided mixed outcomes. The linear (0.8858), non-linear (0.9263), and anaerobic (0.6289) models predicted fast biodegradation, with an estimated primary degradation in ~3.8 days and ultimate mineralization in ~3 weeks.[37] These results indicate that the compound has the potential to degrade relatively quickly under both aerobic and anaerobic conditions.

3.7.4 Implications for environmental safety. The combination of low predicted ecotoxicity and moderate-to-fast biodegradation potential suggests that the designed pyrazolone derivative may not persist in the environment for long periods and is unlikely to cause acute harm to aquatic ecosystems. Nevertheless, the discrepancy between models indicates that it cannot yet be classified as "readily biodegradable" with certainty.[44] For industrial-scale use, especially in systems where discharge to natural water bodies may occur, experimental validation is essential. For industrial-scale applications, particularly in systems where effluents may reach natural water bodies, experimental validation will be a key priority in our future work. We plan to complement the present *in silico* findings with comprehensive laboratory assessments. These include aquatic ecotoxicity assays such as Daphnia magna immobilization, algal growth inhibition, and fish LC_{50} studies to confirm both acute and chronic toxicity predictions. In addition, OECD 301 biodegradability tests will be carried out to experimentally verify the environmental breakdown of the compound. To assess long-term ecological risks, bioaccumulation studies based on $\log K_{ow}$ and bioconcentration factor (BCF) measurements will be performed. Furthermore, soil microbial toxicity studies will be conducted, as corrosion inhibitors may also enter terrestrial ecosystems through sludge disposal. Together, these experimental evaluations will provide a more comprehensive understanding of the compound's environmental safety and will help ensure its responsible and sustainable use in industrial applications.[44,45] The computational results indicate that the C4-substituted heterocyclic pyrazolone is non-toxic to humans and non-ecotoxic *in silico*, with a moderate-to-fast biodegradation profile.

4. Conclusion

This study investigated the corrosion inhibition properties of 3-(5-methyl-3-oxo-2,3-dihydro-1*H*-pyrazol-4-yl)-3-phenylpropanoic

acid (**C4-PRZ-1**) on mild steel in 1 M hydrochloric acid using a combination of experimental and theoretical methods.

•In a 1 M HCl solution, **C4-PRZ-1** demonstrated significant corrosion inhibition of carbon steel (MS). The inhibition efficiency, ascertained using Tafel polarization and electrochemical impedance spectroscopy, exhibited a positive correlation with increasing inhibitor concentration. The potentiodynamic polarization study reveal that (**C4-PRZ-1**) behaved as a mixed type inhibitor.

•Scanning electron microscopy (SEM) coupled with energy-dispersive spectroscopy (EDS) supported the electrochemical findings, confirming the development of a protective coating on the metal surface through physisorption interactions.

•Adsorption studies demonstrated that the interaction of **C4-PRZ-1** with the mild steel surface followed the Langmuir adsorption isotherm.

•Monte Carlo (MC) simulations and density functional theory (DFT) calculations provided theoretical support for the experimental results, illustrating strong adsorption tendencies and electronic interaction of pyrazolone-based molecule with the mild steel substrate.

Conflicts of interest

There are no conflicts to declare.

Data availability

All data supporting this study are provided either in the results and discussion section of this paper.

Acknowledgements

Support for this work by Ibnou Zohr University is gratefully acknowledged. This study did not obtain any external funding.

References

1 I. Aiad, S. M. Shaban, H. Y. Moustapha and A. Hamed, Experimental investigation of newly synthesized gemini cationic surfactants as corrosion inhibitors of mild steel in 1.0 M HCl, *Prot. Met. Phys. Chem. Surfaces*, 2018, **54**, 135–147.

2 H. A. M. A. Hegazy, M. Abdallah and M. Alfakeer, Corrosion Inhibition Performance of a Novel Cationic Surfactant for protection of Carbon Steel Pipeline in Acidic Media, *Int. J. Electrochem. Sci.*, 2018, **13**, 6824–6842.

3 A. Zouitini, Y. Kandri Rodi, H. Elmselem, F. Ouazzani Chahdi, H. Steli, C. Ad, Y. Ouzidan, E. M. Essassi, A. Chetouani and B. Hammouti, Corrosion inhibition behavior of quinoxaline derivative as a green corrosion inhibitor for mild steel in hydrochloric acid: Electrochemical, weight loss and DFT simulations studies, *Moroccan J. Chem.*, 2018, **6**, 391–403.

4 A. G. Bedir, M. Abd El-raouf, S. Abdel-Mawgoud, N. A. Negm and N. M. El Basiony, Corrosion Inhibition of Carbon Steel in Hydrochloric Acid Solution Using Ethoxylated Nonionic Surfactants Based on Schiff Base: Electrochemical and Computational Investigations, *ACS Omega*, 2021, **6**, 4300–4312, DOI: **10.1021/acsomega.0c05476**.

5 D. Djamel, H. Hamani and T. Douadi, Novel heterocyclic quinolone derivatives as green environmental corrosion inhibitors for carbon steel in HCl solution: experimental and theoretical investigation, *J. Adhes. Sci. Technol.*, 2021, **35**, 2319–2345, DOI: **10.1080/01694243.2021.1885923**.

6 H. Ashassi-Sorkhabi, N. Ghalebsaz-Jeddi, F. Hashemzadeh and H. Jahani, Corrosion inhibition of carbon steel in hydrochloric acid by some polyethylene glycols, *Electrochim. Acta*, 2006, **51**, 3848–3854, DOI: **10.1016/j.electacta.2005.11.002**.

7 M. El Achouri, S. Kertit, H. M. Gouttaya, B. Nciri, Y. Bensouda, L. Perez, M. R. Infante and K. Elkacemi, Corrosion inhibition of iron in 1 M HCl by some gemini surfactants in the series of alkanediyl-α,ω-bis-(dimethyl tetradecyl ammonium bromide), *Prog. Org. Coat.*, 2001, **43**, 267–273, DOI: **10.1016/S0300-9440(01)00208-9**.

8 A. N. Senthilkumar, K. Tharini and M. G. Sethuraman, Corrosion inhibitory effect of few piperidine-4-one oximes on mild steel in a hydrochloric medium, *Surf. Rev. Lett.*, 2009, **16**, 141–147, DOI: **10.1142/S0218625X09012408**.

9 J. Aljourani, M. A. Golozar and K. Raeissi, The inhibition of carbon steel corrosion in hydrochloric and sulfuric acid media using some benzimidazole derivatives, *Mater. Chem. Phys.*, 2010, **121**, 320–325, DOI: **10.1016/j.matchemphys.2010.01.040**.

10 R. Hasanzade, S. Bilge, S. Bilgiç, G. Gece and K. Kılıç, Experimental and theoretical calculations on corrosion inhibition of steel in 1 M H_2SO_4 by crown type polyethers, *Corros. Sci.*, 2009, **52**, 984–990, DOI: **10.1016/j.corsci.2009.11.022**.

11 M. Chafiq, A. Chaouiki, H. Lgaz, R. Salghi, S. L. Gaonkar, K. S. Bhat, R. Marzouki, I. A. Ali, M. I. Khan, H. Shimizu and I. M. Chung, Synthesis and corrosion inhibition evaluation of a new Schiff base hydrazone for mild steel corrosion in HCl medium: Electrochemical, DFT, and molecular dynamics stimulations studies, *J. Adhes. Sci. Technol.*, 2020, **34**, 1283–1314, DOI: **10.1080/01694243.2019.1707561**.

12 H. Ashassi-Sorkhabi, A. Kazempour and Z. Frouzat, Superior potentials of hydrazine Schiff bases for efficient corrosion protection of mild steel in 1.0 M HCl, *J. Adhes. Sci. Technol.*, 2021, **35**, 164–184, DOI: **10.1080/01694243.2020.1794357**.

13 I. Kaabi, T. Douadi, D. Daoud, I. Saifi, I. L. Sibous and S. Chafaa, Synthesis characterization and anti-corrosion properties of two new Schiff bases derived from diamino diphenyl ether on carbon steel X48 in 1 M HCl, *J. Adhes. Sci. Technol.*, 2021, **35**, 559–589, DOI: **10.1080/01694243.2020.1816777**.

14 R. W. Revie and H. H. Uhlig, *Corrosion and Corrosion Control. An Introduction to Corrosion Science and Engineering*. 4th edn, John Wiley & Sons, New Jersey, 2008 ISBN: 9780470277270, DOI: **10.1002/9780470277270**.

15 H. H. Khaldoon and S. A. Qasim, Principles, types and applications of corrosion inhibitors operation form metal

and alloys. Review, *AIP Conf. Proc.*, 2023, **2787**, 020002, DOI: 10.1063/5.0148324.

16 P. Zhao, X. Han, W. Wang, M. Zhao and F. Zhang, Exfoliation inhibition on aluminum alloy 7075 by water-soluble phthalocyanine derivates in 1mol/l HCl, *J. Adhes. Sci. Technol.*, 2020, **34**, 1331–1347, DOI: 10.1080/01694243.2019.1707562.

17 M. A. Migahed, Electrochemical investigation of the corrosion behavior of mild steel in 2 M HCl solution in the presence of 1-dodecyl-4-methoxy pyridinium bromide, *Mater. Chem. Phys.*, 2005, **93**, 48–53, DOI: 10.1016/j.matchemphys.2005.02.003.

18 M. Sheydaei, The Use of Plant Extracts as Green Corrosion Inhibitors: A Review, *Surfaces*, 2024, **7**(2), 380–403, DOI: 10.3390/surfaces7020024.

19 B. R. Fazal, T. Becker, B. Kinsella and K. Lepkova, A review of plant extracts as green corrosion inhibitors for CO2 corrosion of carbon steel, *npj Mater. Degrad.*, 2022, **6**, 5, DOI: 10.1038/s41529-021-00201-5.

20 R. M. Bandeira, F. P. Lima, M. S. Nunes, E. C. Dos Santos, J. R. Dos Santos Junior, J. M. Elas de Matos, C. M. Feitosa, M. Rai, S. Bhattarai and D. D. Mulmi, The green plant-based corrosion inhibitors—A sustainable strategy for corrosion protection, *J. Surf. Sci. Technol.*, 2025, **3**, 19, DOI: 10.1007/s44251-025-00084-7.

21 J. Cruz, R. Martĭnez, J. Genesca and E. Garcĭa-Ochoa, Experimental and theoretical study of 1-(2-ethylamino)-2-methylimidazoline as an inhibitor of carbon steel corrosion in acid media, *J. Electroanal.Chem.*, 2004, **566**, 111–121, DOI: 10.1016/j.jelechem.2003.11.018.

22 N. Arrousse, R. Salim, Y. Kaddouri, A. Zarrouk, D. Zahri, F. El Hajjaji, R. Touzani, M. Taleb and S. Jodeh, The inhibition behavior of two pyrimidine-pyrazole derivatives against corrosion in hydrochloric solution: Experimental, surface analysis and *in silico* approach studies, *Arabian J. Chem.*, 2020, **13**, 5949–5965, DOI: 10.1016/j.arabjc.2020.04.030.

23 S. Khan and M. A. Quraish, Synergistic effect of potassium iodide on Inhibition performance of thiadiazoles during corrosion of mild steel in 20% sulfuric acid, *Arab J. Sci. Eng.*, 2010, **35**, 71–82.

24 X. Jiang, Y. G. Zheng and W. Ke, Effect of flow velocity and entrained sand on inhibition performances of two inhibitors for CO_2 corrosion of N80 steel in 3% NaCl solution, *Corros. Sci.*, 2005, **47**, 2636–2658, DOI: 10.1016/j.corsci.2004.11.012.

25 A. Garnica-Rodriguez, J. Genesca, J. Mendoza-Flores and R. Duran-Romero, Electrochemical evaluation of aminotriazole corrosion inhibitor under flow conditions, *J. Appl. Electrochem.*, 2009, **39**(10), 1809–1819, DOI: 10.1007/s10800-009-9884-4.

26 N. Caliskan and E. Akbas, Corrosion inhibition of austenitic stainless steel by some pyrimidine compounds in hydrochloric acid, *Mater. Corros.*, 2012, **63**, 231–237, DOI: 10.1002/maco.201005788.

27 S. El-Maksoud and A. Fouda, Some pyridine derivatives as corrosion inhibitors for carbon steel in an acidic medium, *Mater. Chem. Phys.*, 2005, **93**, 84–90, DOI: 10.1016/j.matchemphys.2005.02.020.

28 J. Aljourani, M. A. Golozar and K. Raeissi, The inhibition of carbon steel corrosion in hydrochloric and sulfuric acid media using some benzimidazole derivatives, *Mater. Chem. Phys.*, 2010, **121**, 320–325, DOI: 10.1016/j.matchemphys.2010.01.040.

29 H. Ashassi-Sorkhab, A. Kazempour and Z. Frouzat, Superior potentials of hydrazine Schiff bases for efficient corrosion protection of mild steel in 1.0 M HCl, *J. Adhes. Sci. Technol.*, 2021, **35**, 164–184, DOI: 10.1080/01694243.2020.1794357.

30 A. M. El Defrawy, M. Abdallah and J. H. Al-Fahemi, Electrochemical and theoretical investigation for some pyrazolone derivatives as inhibitors for the corrosion of C-steel in 0.5 M hydrochloric acid, *J. Mol. Liq.*, 2019, **288**, 110994, DOI: 10.1016/j.molliq.2019.110994.

31 S. A. Mrani, S. El Arrouji, K. Karrouchi, F. El Hajjaji, K. I. Alaoui, Z. Rais and M. Taleb, Inhibitory performance of some pyrazole derivatives against corrosion of mild steel in 1.0 M HCl: Electrochemical, MEB and theoretical studies, *Int. J. Corros. Scale Inhib*, 2018, **7**, 542–569, DOI: 10.17675/2305-6894-2018-7-4-5.

32 G. Laadam, M. El Faydy, F. Benhiba, A. Titi, H. Amegroud, A. S. Al-Gorair, H. Hawsawi, R. Touzani, I. Warad, A. Bellaouchou, A. Guenbour, M. Abdallah and A. Zarrouk, Outstanding anti-corrosion performance of two pyrazole derivatives on carbon steel in acidic medium: Experimental and quantum-chemical examinations, *J. Mol. Liq.*, 2023, **375**, 121268, DOI: 10.1016/j.molliq.2023.121268.

33 Z. Tribak, M. K. Skalli and O. Senhaji, Theoretical Evaluation of the Corrosion Inhibition Performance of an Organic Heterocyclic Compound, Walailak, *JST*, 2021, **18**, 6–9115, DOI: 10.48048/wjst.2021.9115.

34 Y. Ait Elmachkouri, E. Irrou, H. Ouachtak, M. E. Zaki, S. M. Gomha, A. Oubella and M. L. Taha, In-silico studies of Pyrazolopyranopyrimidine as a Potential Anticancer Inhibitor: Synthesis, Network Pharmacology, ADMET Prediction, Molecular Docking, and Dynamics Simulations, *J. Mol. Struct.*, 2025, 142829.

35 E. Świętczak, M. Rachwalski and A. M. Pieczonka, Eco-friendly methods for the synthesis of N-acyl pyrazole derivatives with luminescent properties, *RSC Adv.*, 2025, **15**(16), 12698–12703.

36 D. Becerra and J. C. Castillo, Recent advances in the synthesis of anticancer pyrazole derivatives using microwave, ultrasound, and mechanochemical techniques, *RSC Adv.*, 2025, **15**(9), 7018–7038.

37 Y. Ait Elmachkouri, E. Irrou, J. T. Mague, A. Oubella, M. T. Rehman, M. F. AlAjmi and M. L. Taha, Design, Synthesis, and Crystal Structure of New C5-Substituted Pyrazolopyranopyrimidines: *In Silico* Studies Based on Network Pharmacology as Promising Anticancer Candidates for Lung Cancer, *J. Mol. Struct.*, 2025, 142800.

38 K. H. Rashid, K. F. AL-Azawi, A. A. Khadom, A. S. Jasim and M. M. Kadhim, New pyrazole derivative as effective corrosion

inhibitor for carbon steel in 1 M HCl: experimental and theoretical analysis, *J. Mol. Struct.*, 2023, **1287**, 135661.

39 A. M. Ashmawy, M. A. Mostafa, A. B. Kamal, G. A. Ali and M. S. A. El-Gaby, Corrosion inhibition of mild steel in 1 M HCl by pyrazolone-sulfonamide hybrids: synthesis, characterization, and evaluation, *Sci. Rep.*, 2023, **13**(1), 18555.

40 A. M. El Defrawy, M. Abdallah and J. H. Al-Fahemi, Electrochemical and theoretical investigation for some pyrazolone derivatives as inhibitors for the corrosion of C-steel in 0.5 M hydrochloric acid, *J. Mol. Liq.*, 2019, **288**, 110994.

41 M. A. Deyab, Solfunium-based ionic liquid as an anticorrosive agent for thermal desalination units, *J. Mol. Liq.*, 2019, **296**, 111742, DOI: **10.1016/j.molliq.2019.111742**.

42 D. Prasad, R. Singh, S. Kaya and B. El Ibrahimi, Natural corrosion inhibitor of renewable eco-waste for SS-410 in sulfuric acid medium: adsorption, electrochemical, and computational studies, *J. Mol. Liq.*, 2022, **351**, 118671, DOI: **10.1016/j.molliq.2022.118671**.

43 F. EL Hajjaji, E. Ech-chihbi, R. Salim, A. Titi, M. Messali, B. El Ibrahimi, S. Kaya and M. Taleb, A detailed electronic-scale DFT modeling/MD simulation, electrochemical and surface morphological explorations of imidazolium-based ionic liquids as sustainable and nontoxic corrosion inhibitors for mild steel in 1 M HCl, *J. Mater. Sci. Eng. B*, 2023, **289**, 116232, DOI: **10.1016/j.mseb.2022.116232**.

44 Y. Ait Elmachkouri, E. Irrou, A. A. Thiruvalluvar, E. H. Anouar, V. Varadharajan, H. Ouachtak and M. L. Taha, Synthesis, Crystal structure, spectroscopic characterization, DFT calculations, Hirshfeld surface analysis, molecular docking, and molecular dynamics simulation investigations of novel pyrazolopyranopyrimidine derivatives, *J. Biomol. Struct. Dyn.*, 2024, **42**, 1–19, DOI: **10.1080/07391102.2023.2268187**.

45 Y. Ait Elmachkouri, Y. Sert, E. Irrou, E. H. Anouar, H. Ouachtak, J. T. Mague and M. L. Taha, Synthesis, X-ray Diffraction, Spectroscopic Characterization, Hirshfeld Surface Analysis, Molecular Docking Studies, and DFT Calculation of New Pyrazolone Derivatives, *Polycyclic Aromat. Compd.*, 2023, 1–22, DOI: **10.1080/10406638.2023.2219804**.

46 A. Ramachandran, P. Anitha and S. Gnanavel, Structural and electronic impacts on corrosion inhibition activity of novel heterocyclic carboxamides derivatives on mild steel in 1 M HCl environment: Experimental and theoretical approaches, *J. Mol. Liq.*, 2022, **359**, 119218, DOI: **10.1016/j.molliq.2022.119218**.

47 M. Chadili, M. M. Rguiti, B. El Ibrahimi, R. Oukhrib, A. Jmiai, M. Beelkhaouda, L. Bammou, M. Hilali and L. Bazzi, Corrosion Inhibition of 3003 Aluminum Alloy in Molar Hydrochloric Acid Solution by Olive Oil Mill Liquid By-Product, *Int. J. Corros.*, 2021, 6662395, DOI: **10.1155/2021/6662395**.

48 S. Dahiya, S. Lata, R. Kumar and O. S. Yadav, Comparative performance of Uroniums for controlling corrosion of steel with methodical mechanism of inhibition in acidic medium: part1, *J. Mol. Liq.*, 2016, **221**, 124–132, DOI: **10.1016/j.molliq.2016.05.073**.

49 N. Ashwini, S. Shakeel Nawaz, D. Ramakrishna and S. Ranganatha, Inhibition of mild steel corrosion by 4-[(benzylidene)-amino]-antipyrine, *Results Surf. Interfaces*, 2024, **15**, 100209, DOI: **10.1016/j.rsurfi.2024.100209**.

50 A. S. Yaro and H. F. Ibraheem, The Inhibition Effect of Peach Juice on Corrosion of Low Carbon Steel in Hydrochloric Acid at Different Temperatures, *Iraqi J. Chem. Pet. Eng.*, 2010, **11**(1), 65–76, DOI: **10.31699/IJCPE.2010.1.8**.

51 A. Kartika Madurani, S. Firdausi, H. Harmami, I. Ulfin, E. Shinchi, S. Rinda Sari, M. Tominaga and F. Kurniawan, Improving inhibition efficiency of 304 stainless steel using an organic extract in acidic and high temperature environment: Experimental and theoretical studies, *Appl. Surf. Sci. Adv.*, 2024, **22**, 100620, DOI: **10.1016/j.apsadv.2024.100620**.

52 D. Quy Huong, T. Duong and P. C. Nam, Effect of the Structure and Temperature on Corrosion Inhibition of Thiourea Derivatives in 1.0 M HCl Solution, *ACS Omega*, 2019, **4**(11), 14478–14489, DOI: **10.1021/acsomega.9b01599**.

53 Y. Chen, K. Wippermann, C. Rodenbücher, Y. Suo and C. Korte, Impedance Analysis of Capacitive and Faradaic Processes in the Pt/[Dema][TfO] Interface, *ACS Appl. Mater. Interfaces*, 2024, **16**(4), 5278–5285, DOI: **10.1021/acsami.3c15465**.

54 K. Ismail and W. Badawy, Electrochemical and XPS investigations of cobalt in KOH solutions, *J. Appl. Electrochem.*, 2000, **30**, 1303–1311, DOI: **10.1023/A:1026560422090**.

55 S. S. Abdel-Rehim, K. F. Khaled and N. A. Al-Mobarak, Corrosion inhibition of iron in hydrochloric acid using pyrazole, *Arabian J. Chem.*, 2011, **4**(3), 333–337, DOI: **10.1016/j.arabjc.2010.06.056**.

56 E. A. Sahin, F. Tezkan, R. Solmaz and G. Kardas, Inhibitive effect of 4-amino-N-benzylidene-benzamide Schiff base on mild steel corrosion in HCl solution, *J. Adhes. Sci. Technol.*, 2020, **34**(2), 135–152, DOI: **10.1080/01694243.2019.1662202**.

57 H. Hamani, T. Douadi, D. El Daoud, M. Al-Noaimi, R. A. Rikkouh and S. Chafaa, 1-(4-Nitrophenylo-imino)-1-(phenylhydrazono)-propan-2-one as corrosion inhibitor for mild steel in 1 M HCl solution: weight loss, electrochemical, thermodynamic and quantum chemical studies, *J. Electroanal. Chem.*, 2017, **801**, 425–438, DOI: **10.1016/j.jelechem.2017.08.031**.

58 S. Jayakumar, T. Nandakumar, M. Vadivel, C. Thinaharan, R. P. George and J. Philip, Corrosion inhibition of mild steel in 1 M HCl using Tamarindus indica extract: electrochemical, surface and spectroscopic studies, *J. Adhes. Sci. Technol.*, 2020, **34**(7), 713–743, DOI: **10.1080/01694243.2019.1681156**.

59 L. Boucherit, T. Douadi, N. Chafai, M. Al-Noaimi and S. Chafaa, The inhibition activity of 1, 10-bis (2-formyl-phenyl)- 1, 4, 7, 10-tetraoxadecane (Ald) and its Schiff base (L) on the corrosion of carbon steel in HCl: Experimental and theoretical studies, *Int. J. Electrochem. Sci.*, 2018, **13**(4), 3997–4025, DOI: **10.20964/2018.04.59**.

60 R. A. Rikkouh, T. Douadi, H. Hamani, M. Al-Noaimi and S. Chafaa, Inhibition effect of 4, 4'-thio bis{ N-[(E) –phenol-3-ylmethylidene] aniline} on the corrosion of mild steel in HCl solution under stagnant condition and hydrodynamic flow, *J. Adhes. Sci. Technol.*, 2020, **34**(13), 1454–1479, DOI: **10.1080/01694243.2019.1708671**.

61 X. Li, X. Xie, S. Deng and G. Du, Two phenylpyrimidine derivatives as new corrosion inhibitors for cold rolled steel in hydrochloric acid solution, *Corros. Sci.*, 2014, **87**, 27–39, DOI: **10.1016/j.corsci.2014.05.017**.

62 R. Solmaz, Investigation of adsorption and corrosion inhibition of mild steel in hydrochloric acid solution by 5-(4 Dimethylaminobenzylidene) rhodamine, *Corros. Sci.*, 2014, **79**, 169–176, DOI: **10.1016/j.corsci.2013.11.001**.

63 A. Zarrouk, H. Zarrok, Y. Ramli, M. Bouachrine, B. Hammouti, A. Sahibed-dine and F. Bentiss, Inhibitive properties, adsorption, and theoretical study of 3, -dimethyl-1-(prop-2-yn-1-yl) quinoxaline-2 (1H)-one as efficient corrosion inhibitor for carbon steel in hydrochloric acid solution, *J. Mol. Liq.*, 2016, **222**, 239–252, DOI: **10.1016/j.molliq.2016.07.046**.

64 A. Kokalj, on the estimation of standard adsorption free energy from corrosion inhibition efficiencies, *Corros. Sci.*, 2023, **217**, 111139, DOI: **10.1016/j.corsci.2023.111139**.

65 A. S. Fouda, K. Shalabi and R. Ezzat, Evaluation of some thiadiazole derivatives as acid corrosion inhibitors for carbon steel in aqueous solutions, *J. Mater. Environ. Sci.*, 2015, **6**, 1022–1039.

66 O. H. Pakarinen, J. M. Mativetsky, A. Gulans, M. J. Puska, A. S. Foster and P. Grutter, Role of van der Waals forces in the adsorption and diffusion of organic molecules on an insulating surface, *Phys. Rev. B:Condens. Matter Mater. Phys.*, 2009, **80**, 085401, DOI: **10.1103/PhysRevB.80.085401**.

67 H. Shao, X. Yin, K. Zhang, W. Yang, Y. Chen and Y. Liu, N-[2-(3-indolyl)ethyl]-cinnamamide synthesized from Cinnamomum cassia presl and alkaloid tryptamine as green corrosion inhibitor for Q235 steel in acidic medium, *J. Mater. Res. Technol.*, 2022, **20**, 916–933, DOI: **10.1016/j.jmrt.2022.07.122**.

68 A. R. Shahmoradi, M. Ranjbarghanei, A. A. Javidparvar, L. Guo, E. Berdimurodov and B. Ramezanzadeh, Theoretical and surface/electrochemical investigations of walnut fruit green husk extract as an effective inhibitor for mild-steel corrosion in 1 M HCl electrolyte, *J. Mol. Liq.*, 2021, **338**, 116550, DOI: **10.1016/j.molliq.2021.116550**.

69 H. R. Hsissou, O. Dagdag, S. About, F. Benhiba, M. Berradi, M. El Bouchti, A. Berisha, N. Hajjaji and A. Elhar, Novel derivative epoxy resin TGETET as a corrosion inhibition of E24 carbon steel in 1.0 M HCl solution. Experimental and computational (DFT and MD simulations) methods, *J. Mol. Liq.*, 2019, **284**, 182–192, DOI: **10.1016/j.molliq.2019.03.180**.

70 N. Idlahoussaine, M. Lasri, R. Idouhli, W. Daoudi, B. EL Ibrahimi, E. Berdimurodov, M. El Ouardi, A. Ait Addi, N. Aliev, A. EL Aatiaoui and A. Abouelfida, Imidazole/pyridine-based derivative as a novel protectivity agent for mild steel corrosion in acidic solution: Comprehensive investigations, *J. Mol. Struct.*, 2024, 137705, DOI: **10.1016/j.molstruc.2024.137705**.

71 I. B. Obot, S. A. Umoren, Z. M. Gasem, R. Suleiman and B. El Ali B, Theoretical prediction and electrochemical evaluation of vinyl imidazole and allyl imidazole as corrosion inhibitors for mild steel in 1 M HCl, *J. Ind. Eng. Chem.*, 2015, **21**, 1328–1339, DOI: **10.1016/j.jiec.2014.05.049**.

72 K. S. M. Ferigita, M. G. K. Al-Falah, M. Saracoglu, Z. Kokbudak, S. Kaya, M. O. Abdels Alaghani and F. Kandemirli, Corrosion behavior of new oxo-pyrimidine derivatives on mild steel in acidic media: Experimental, surface characterization, theoretical, and Monte Carlo studies, *Appl. Surf. Sci. Adv.*, 2022, **7**, 100200, DOI: **10.1016/j.apsadv.2021.100200**.

73 S. Sengupta, M. Murmu, S. Mandal, H. Hirani and P. Banerjee, Competitive corrosion inhibition performance of alkyl/acyl substituted 2-(2-hydroxybenzylideneamino) phenol protecting mild steel used in adverse acidic medium: A dual approach analysis using FMOs/molecular dynamics simulation corroborated experimental fin, *Colloids Surfaces A Physicochem. Eng. Asp.*, 2021, **617**, 126314, DOI: **10.1016/j.colsurfa.2021.126314**.

74 V. K. Shenoy, P. P. Venugopal, P. D. Reena Kumari and D. Chakraborty, Anti-corrosion investigation of a new nitro veratraldehyde substituted imidazopyridine derivative Schiff base on mild steel surface in hydrochloric acid medium: experimental, computational, surface morphological analysis, *Mater. Chem. Phys.*, 2022, **281**, 125855, DOI: **10.1016/j.matchemphys.2022.125855**.

75 F. El-Dossoki, S. Abedelhady, M. Abedalhmeed, M. Abdel-Raouf and A. Ali, Micellization properties, molal volume and polarizability of newly synthesized gemini-cationic surfactants, Egypt, *J. Chem.*, 2022, **65**, 585–599, DOI: **10.21608/EJCHEM.2021.71993.4507**.

76 H. M. Abd El-Lateef, S. Shaaban, M. M. Khalaf, A. Toghan and K. Shalabi, Synthesis, experimental, and computational studies of water-soluble anthranilic organoselenium compounds as safe corrosion inhibitors for J55 pipeline steel in acidic oilfield formation water, *Colloids Surf. A Physicochem. Eng. Asp.*, 2021, **625**, 126894, DOI: **10.1016/j.colsurfa.2021.126894**.

77 A. Toghan, H. S. Gadow, H. M. Dardeer and H. M. Elabbasy, New promising halogenated cyclic imides derivatives as potential corrosion inhibitors for carbon steel in hydrochloric acid solution, *J. Mol. Liq.*, 2021, **325**, 115136, DOI: **10.1016/j.molliq.2020.115136**.

78 S. Satpati, A. Suhasaria, S. Ghosal, A. Saha, S. Dey and D. Sukul, Amino acid, and cinnamaldehyde conjugated Schiff bases as proficient corrosion inhibitors for mild steel in 1 M HCl at higher temperature and prolonged exposure: Detailed electrochemical, adsorption and theoretical study, *J. Mol. Liq.*, 2021, **324**, 115077, DOI: **10.1016/j.molliq.2020.115077**.